A NUMERICAL STUDY OF UNSTEADY, THERMAL, GLASS FIBER DRAWING PROCESSES *

HONG ZHOU † AND M. GREGORY FOREST ‡

Abstract. An efficient second-order stable numerical method is presented to solve the model partial differential equations of thermal glass fiber processing. The physical process and structure of the model equations are described first. The numerical issues are then clarified. The heart of our method is a MacCormack scheme with flux limiting. The numerical method is validated on a linearized isothermal model and by comparison with known exact stationary solutions. The numerical method is then generalized to solve the equations of motion of thermal glass fiber drawing, exhibiting order of convergence. Further, the nonlinear PDE scheme is benchmarked against an independent linearized stability analysis of boundary value solutions near the onset of instability, which demonstrates the efficiency of the method.

Key words. MacCormack scheme, flux limiting, thermal glass fiber drawing.

MSC 2000 subject classifications. 35M99, 35Q35, 65N06.

1. Introduction

Optical fibers are thin cylindrical dielectric waveguides used to send light energy for communication. Optical fibers have a number of advantages over copper-based electrical signal transmission. For example, glass optical fiber is immune to electromagnetic interference, such as is caused by thunderstorms, and has a much wider bandwidth. The issue of interest for this paper is the actual production process for glass fibers.

Fiber drawing begins by heating the tip of the *preform* (the solid rod from which fibers are drawn) to a molten state and allowing it to extend downward under the force of gravity while shrinking in diameter into a fine-diameter filament. These conditions correspond to upstream boundary conditions on fiber radius, velocity and temperature. A pulling and winding mechanism sustains a drawing force, which corresponds to a downstream boundary condition. The equations and attendant boundary conditions are given in section 2. Interior to the steady process is a free boundary of liquid-to-glass transition.

Extensive research has been done on the drawing process of glass fibers (for example, Glicksman [10], Geyling and Homsy [9]). The governing model equations of a slender glass fiber drawing process consist of a system of nonlinear partial differential equations in one space dimension (along the fiber axis) and time. The equations cannot be simply classified as elliptic, hyperbolic or parabolic, and the structure varies with the assumed physics. Most previous studies on glass fiber drawing processes deal with steady solutions, in which case one only needs to solve a set of ordinary differential equations with appropriate boundary conditions. However, from a practical standpoint, it is of significant interest to simulate the unsteady or transient process of glass fiber drawing, for example to investigate the sources of diameter variations, or to assess stability of a given process. To do so, one has to solve the full set of partial differential equations. Due to the nonstandard structure of the governing equations, an efficient numerical method has to be developed, rather than simply adopted from the

†Department of Applied Mathematics, Naval Postgraduate School, Monterey, CA 93943-5216 (hzhou@nps.navy.mil).

‡Department of Mathematics, University of North Carolina, Chapel Hill, NC 27599-3250.

existing literature. As one varies the dominant physics, the mathematical structure of the model equations varies [1], and the numerical algorithm likewise has to accommodate this structure. For viscoelastic fluids, Beris and Liu [3, 14], Forest and Wang [6], have developed algorithms where the differential operator (in one space dimension and time) is quasi-linear first order, for which an explicit nonlinear classification is provided by characteristic analysis. For the optical fiber model below, the quasi-linear part of the differential operator has an elliptic space-time component (which is itself ill-posed), and viscosity terms provide the regularizer; Eggers and Dupont [5] have developed an algorithm for an isothermal viscous fluid model, some features of which are adopted here.

The aim of this paper is to present an efficient numerical method for solving the governing model equations of slender glass fibers. This model is robust enough to accommodate anticipated variations in the governing physics and rheology. Detailed simulations of glass fiber processing and comparisons with experiments have been presented elsewhere [7], although exemplary simulations are included here.

In the following sections a brief discussion of the governing equations is given, and different numerical methods are compared with application to a simple model problem. Then we outline our method to solve the governing model equations for glass fibers. Numerical experiments are presented, demonstrating the efficiency of our method. The paper ends with some numerical results on the glass fiber drawing process.

2. The equations of motion

To model the glass fiber preform drawing process, one typically takes advantage of the fact that the fiber is slender and uses asymptotic theory to obtain a *quasi-one-dimensional* approximation [1, 4, 9, 16, 17]. In this approach, leading order descriptions of the free surface radius ϕ, the axial velocity v, pressure p, and temperature T are derived which depend only on the axial coordinate z and time t. These slender fiber models have proven extremely valuable in isolating coupled phenomena in systems of one-dimensional nonlinear PDEs, from which one can extract significant physical information and develop accurate codes.

The leading order dimensionless quasi-1D model equations for axisymmetric filaments consist of the continuity equation, balance of linear momentum, and energy equation [7, 8]:

$$\begin{cases} (\phi^2)_t + (v\phi^2)_z = 0, \\\\ (\phi^2 v)_t + (\phi^2 v^2)_z = \frac{1}{F}\phi^2 + \frac{1}{W}\phi_z + [\phi^2\eta(T)v_z]_z, \\\\ T_t + vT_z = \frac{H}{\phi}(T_{wall}^4 - T^4) - 2St\phi^{-1}[(v\phi)^m\phi^{-1}](T - T_a), \end{cases} \tag{2.1}$$

where $z \in [0,1]$, $m = 1/3$, and the temperature-dependent dimensionless viscosity $\eta(T)$ is

$$\eta(T) = \exp\left[\alpha(\frac{1}{T} - \beta)\right]. \tag{2.2}$$

Here F and W are the Froude and Weber numbers, which respectively parametrize gravity and surface tension relative to inertia; St is the Stanton number, representing the dimensionless heat transfer coefficient; H is the effective radiative transfer coefficient for the surface of the fiber; T_{wall} is the temperature of the furnace; T_a is

the ambient air temperature. The furnace temperature T_{wall} may vary in the axial direction. One can also use a nonconstant ambient temperature T_a to simulate the heating zone and cooling zone. In this study we simply treat both T_{wall} and T_a as constants.

The boundary conditions are given as follows:
- Upstream boundary conditions:

$$\phi(0) = 1, v(0) = 1, T(0) = 1.$$

- Downstream boundary conditions:

$$v(1) = Dr \, (\text{draw ratio}).$$

Let

$$\mathbf{w} = \begin{bmatrix} \phi^2 \\ \phi^2 v \\ T \end{bmatrix}, \tag{2.3}$$

then the equations we will solve can be put in a general form

$$\mathbf{w}_t = -A(\mathbf{w})\mathbf{w}_z + M(\mathbf{w}) + NL(\mathbf{w}_z) + [G(\mathbf{w})\mathbf{w}_z]_z, \tag{2.4}$$

where

$$A(\mathbf{w}) = \begin{bmatrix} 0 & 1 & 0 \\ -v^2 - \frac{1}{2W\phi} & 2v & 0 \\ 0 & 0 & v \end{bmatrix}, \tag{2.5}$$

and $NL(\mathbf{w}_z)$ is a nonlinear function of $\mathbf{w}_z$, $M(\mathbf{w})$ and $G(\mathbf{w})$ are some functions of $\mathbf{w}$. The three eigenvalues of A are

$$\lambda = v \pm \sqrt{-\frac{1}{2W\phi}}, v. \tag{2.6}$$

So the system (2.1) is a second-order PDE, whose first two equations would form an elliptic system if viscosity were ignored. This classical Hadamard instability behavior in the absence of viscosity comes from *Rayleigh instability* [2, 6, 18]. The Rayleigh instability tells us that a fluid jet with uniform radius and constant velocity will break up due to the surface tension induced growth of perturbation. Therefore, the viscous terms in (2.1) are necessary to make the initial value problem well-posed.

In the absence of viscosity, the system (2.1) in our study here is elliptic type everywhere (that is, it is elliptic for all values of v and ϕ). The viscosity is necessary to regularize the system. In other systems, for example, the PDE describing the isothermal evolution of a compressible fluid [12], the PDE is of mixed-type (that is, in some regions of solution value, it is elliptic; in other regions, it is hyperbolic). For such PDEs, weak solutions can be properly defined by adding relaxation regulation. Jin [12] has designed a robust total-variation-diminishing (TVD) method for solving mixed-type PDEs. However, the PDE system in our study is not mixed-type. The initial value problem we study here is well-posed and our numerical method works only for positive viscosity. We also note that our numerical method cannot be applied to solve mixed-type PDEs.

If one assumes that viscosity dominates and thereby ignores the effects of fluid inertia, surface tension, and gravity, then the system (2.1) is reduced to (set $m = 1/3$)

$$(\phi^2)_t + (v\phi^2)_z = 0, \tag{2.7}$$

$$\left[\phi^2 \eta(T) v_z\right]_z = 0, \tag{2.8}$$

$$T_t + vT_z = \frac{H}{\phi}(T_{wall}^4 - T^4) - 2St\,\frac{1}{\phi^{5/3}}\,v^{1/3}(T - T_a), \tag{2.9}$$

whose steady state solutions and their linearized stability have been studied by Geyling and Homsy [9]. Dewynne, Ockendon and Wilmott [4] also studied the same reduced model where the energy equation (2.9) is not included but the viscosity η is assumed to be a function of z or t only. Under these assumptions, they have found exact solutions. Schultz and Davis [17] have studied steady solutions of isothermal thin fiber models.

To our knowledge, the present paper is the first one to study the full equations (2.1) and (2.2). We now focus our attention on numerical methods for the model (2.1) and (2.2).

3. A preliminary study of numerical methods

In this section we compare several numerical methods with application to a simple model. This study will shed light on the numerical solution of (2.1).

Let us consider a simplified linear system of isothermal equations as follows:

$$\phi_t + \phi_z + v_z = 0, \tag{3.1}$$

$$v_t - \phi_z + v_z = v_{zz}, \tag{3.2}$$

where $z \in [0,1]$, and the boundary conditions are

$$\phi(0) = 1, v(0) = 1, v(1) = 1.5. \tag{3.3}$$

By rewriting it as

$$\begin{bmatrix} \phi \\ v \end{bmatrix}_t + \begin{bmatrix} 1 & 1 \\ -1 & 1 \end{bmatrix} \begin{bmatrix} \phi \\ v \end{bmatrix}_z = \begin{bmatrix} 0 \\ v \end{bmatrix}_{zz}, \tag{3.4}$$

it is easy to see that this simple system is similar to (2.1) in the sense that they both contain viscosity terms and would be elliptic if viscosity were absent.

To investigate the well-posedness of the initial value problem of (3.4), we consider solutions of (3.4) of the form $\phi = \exp(ikz)f_1(t)$ and $v = \exp(ikz)f_2(t)$. Then the system (3.4) yields

$$f_1'(t) + ik\,f_1(t) + ik\,f_2(t) = 0, \tag{3.5}$$

$$f_2'(t) + ik\,f_2(t) - ik\,f_1(t) = -k^2 f_2(t), \tag{3.6}$$

or in vector form,

$$\frac{d}{dt}\begin{bmatrix} f_1(t) \\ f_2(t) \end{bmatrix} = -ik\begin{bmatrix} 1 & 1 \\ -1 & 1-ik \end{bmatrix} \begin{bmatrix} f_1(t) \\ f_2(t) \end{bmatrix} \equiv B\begin{bmatrix} f_1(t) \\ f_2(t) \end{bmatrix}. \tag{3.7}$$

The eigenvalues of the matrix B are given by

$$\lambda_{1,2} = -ik - \frac{k^2}{2} \pm k\sqrt{\frac{k^2}{4} + 1}, \tag{3.8}$$

whose real parts are bounded by

$$\mathrm{Re}(\lambda_1) = -\frac{k^2}{2} - k\sqrt{\frac{k^2}{4}+1} \leq 0, \tag{3.9}$$

$$\mathrm{Re}(\lambda_2) = k\left(-\frac{k}{2} + \sqrt{\frac{k^2}{4}+1}\right) = \frac{k}{\frac{k}{2}+\sqrt{\frac{k^2}{4}+1}} \leq \frac{k}{\frac{k}{2}+\frac{k}{2}} = 1, \tag{3.10}$$

respectively. This simple analysis shows that the solution of the initial value problem of (3.4) depends continuously on the data.

The exact steady state solution of (3.4) with boundary conditions (3.3) is

$$v_0(z) = \frac{1}{e^2-1}(0.5e^{2z}+e^2-1.5), \tag{3.11}$$

$$\phi_0(z) = 2-v_0(z) = \frac{1}{e^2-1}(e^2-0.5-0.5e^{2z}). \tag{3.12}$$

To study the stability of the steady state solution, we consider the evolution of perturbations to the steady state. Substituting $\tilde{\phi}(z,t) = \phi_0(z) + \phi(z,t)$ and $\tilde{v}(z,t) = v_0(z) + v(z,t)$ into (3.3) and (3.4), we obtain that perturbations $\phi(z,t)$ and $v(z,t)$ satisfy

$$\begin{cases} \phi_t = -\phi_z - v_z, & \phi(0) = 0, \\ v_t = \phi_z - v_z + v_{zz}, & v(0) = v(1) = 0. \end{cases} \tag{3.13}$$

Let

$$g(t) = \int_0^1 e^{-2z}\left[\frac{(\phi(z,t))^2}{2} + \frac{(v(z,t))^2}{2}\right]dz. \tag{3.14}$$

We are going to show that $g(t)$ is non-increasing. Taking the derivative with respect to t, we get

$$\begin{aligned}\frac{dg(t)}{dt} &= \int_0^1 e^{-2z}[\phi\phi_t + vv_t]dz \\ &= \int_0^1 e^{-2z}[\phi(-\phi_z-v_z) + v(\phi_z-v_z+v_{zz})]dz \\ &= \int_0^1 e^{-2z}\left[-(\frac{\phi^2}{2})_z - 2\phi v_z + (v\phi)_z - (\frac{v^2}{2})_z + (vv_z)_z - (v_z)^2\right]dz. \end{aligned} \tag{3.15}$$

Here we have used (3.4) and the two relations below:

$$v\phi_z = (v\phi)_z - \phi v_z, \tag{3.16}$$

$$vv_{zz} = (vv_z)_z - (v_z)^2. \tag{3.17}$$

Rearranging terms leads to

$$\frac{dg(t)}{dt} = \int_0^1 e^{-2z}\left[-\frac{\phi^2}{2}+v\phi-\frac{v^2}{2}+vv_z\right]_z dz + \int_0^1 e^{-2z}\left[-2\phi v_z - (v_z)^2\right]dz. \tag{3.18}$$

Applying integration by parts to the first integral and using the boundary conditions $\phi(0)=v(0)=v(1)=0$, we obtain

$$\frac{dg(t)}{dt}=-\frac{e^{-2}}{2}\left[\phi(1)\right]^2+\int_0^1 e^{-2z}\left[-\phi^2+2v\phi-v^2+2vv_z\right]dz$$

$$+\int_0^1 e^{-2z}\left[-2\phi v_z-(v_z)^2\right]dz,$$

$$=-\frac{e^{-2}}{2}\left[\phi(1)\right]^2-\int_0^1 e^{-2z}\left[\phi-v+v_z\right]^2dz\leq 0. \tag{3.19}$$

Thus $g(t)$ is non-increasing, indeed decreasing unless all perturbations vanish. This implies that the perturbations are decreasing until the steady state is reached, so that the steady state solution is stable. Numerical experiments confirm that the perturbations decrease with time and the steady state is stable.

Now we compare several different numerical methods and their corresponding results for this simple system. For simplicity, we use the predictor-corrector method for time-integration in all the methods presented in this section.

Divide time into intervals of length Δt and let $\Delta z=1/N$ be the spatial increment. Let ϕ_j^n approximate the solution $\phi(j\Delta z,n\Delta t)$ and v_j^n approximate the solution $v(j\Delta z,n\Delta t)$.

One-sided first order method
This one-sided first order method is motivated by upwind differences in the velocity direction. It is given by

$$Predictor: \begin{cases} \phi_j^* = \phi_j^n - \dfrac{\Delta t}{\Delta z}(\phi_j^n - \phi_{j-1}^n) - \dfrac{\Delta t}{\Delta z}(v_j^n - v_{j-1}^n) \\[3mm] v_j^* = v_j^n + \dfrac{\Delta t}{\Delta z}(\phi_j^n - \phi_{j-1}^n) - \dfrac{\Delta t}{\Delta z}(v_j^n - v_{j-1}^n) + \dfrac{\Delta t}{(\Delta z)^2}(v_{j+1}^n - 2v_j^n + v_{j-1}^n) \end{cases} \tag{3.20}$$

$$Corrector: \begin{cases} \phi_j^{n+1} = \dfrac{\phi_j^n + \phi_j^*}{2} - \dfrac{\Delta t}{2\Delta z}(\phi_j^* - \phi_{j-1}^*) - \dfrac{\Delta t}{2\Delta z}(v_j^* - v_{j-1}^*) \\[3mm] v_j^{n+1} = \dfrac{v_j^n + v_j^*}{2} + \dfrac{\Delta t}{2\Delta z}(\phi_j^* - \phi_{j-1}^*) - \dfrac{\Delta t}{2\Delta z}(v_j^* - v_{j-1}^*) \\[3mm] \qquad + \dfrac{\Delta t}{2(\Delta z)^2}(v_{j+1}^* - 2v_j^* + v_{j-1}^*) \end{cases} \tag{3.21}$$

where $j=2,\cdots,N$. The boundary conditions are

$$\phi_1^n = \phi_1^* = 1, v_1^n = v_1^* = 1, v_{N+1}^n = v_{N+1}^* = 1.5. \tag{3.22}$$

In Figure 3.1 we show the difference between the numerical solution at time $= 5.0$ with 80 grid points in $[0,1]$ and the exact steady state solution. The initial conditions are $\phi=1$ for $z\in[0,1]$, $v=1$ for $z\in[0,1)$ and $v=1.5$ at $z=1$.
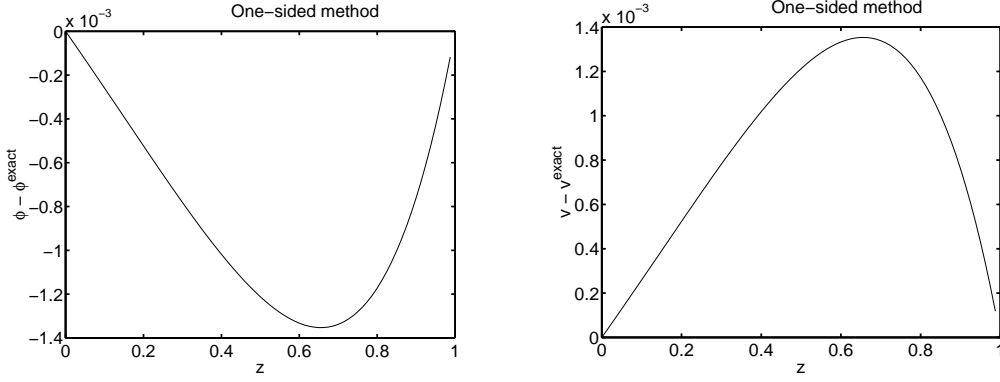
FIG. 3.1. *Error of one-sided first order method.*

Central-differencing method

$$
Predictor: \begin{cases} \phi_j^* = \phi_j^n - \dfrac{\Delta t}{2\Delta z}(\phi_{j+1}^n - \phi_{j-1}^n) - \dfrac{\Delta t}{2\Delta z}(v_{j+1}^n - v_{j-1}^n) \\[2mm] v_j^* = v_j^n + \dfrac{\Delta t}{2\Delta z}(\phi_{j+1}^n - \phi_{j-1}^n) - \dfrac{\Delta t}{2\Delta z}(v_{j+1}^n - v_{j-1}^n) \\[2mm] \qquad + \dfrac{\Delta t}{(\Delta z)^2}(v_{j+1}^n - 2v_j^n + v_{j-1}^n) \end{cases} \tag{3.23}
$$

$$
Corrector: \begin{cases} \phi_j^{n+1} = \dfrac{\phi_j^n + \phi_j^*}{2} - \dfrac{\Delta t}{4\Delta z}(\phi_{j+1}^* - \phi_{j-1}^*) - \dfrac{\Delta t}{4\Delta z}(v_{j+1}^* - v_{j-1}^*) \\[2mm] v_j^{n+1} = \dfrac{v_j^n + v_j^*}{2} + \dfrac{\Delta t}{4\Delta z}(\phi_{j+1}^* - \phi_{j-1}^*) - \dfrac{\Delta t}{4\Delta z}(v_{j+1}^* - v_{j-1}^*) \\[2mm] \qquad + \dfrac{\Delta t}{2(\Delta z)^2}(v_{j+1}^* - 2v_j^* + v_{j-1}^*) \end{cases} \tag{3.24}
$$

where $j = 2, \cdots, N$. The boundary conditions are

$$
\phi_1^n = \phi_1^* = 1, v_1^n = v_1^* = 1, v_{N+1}^n = v_{N+1}^* = 1.5. \tag{3.25}
$$

Additional boundary conditions are needed at the "ghost grid" for ϕ_{N+1}^n and ϕ_{N+1}^*, obtained by extrapolation:

$$
\phi_{N+1}^n = 2\phi_N^n - \phi_{N-1}^n, \phi_{N+1}^* = 2\phi_N^* - \phi_{N-1}^*. \tag{3.26}
$$

Figure 3.2 depicts the error of the central differencing method, where the initial conditions, final time and mesh size are chosen the same as in Figure 3.1. Clearly, the central differencing method exhibits wild oscillations even though it is more accurate than the one-sided first order method. Due to the presence of viscosity in the equation of v, the oscillation of the error of v is smeared and hence less dramatic than that of ϕ. As will be seen in comparing Fig. 3.2 and Fig. 3.5, oscillatory error at the

numerical error level, although not fatal, does contribute to a significant increase in the magnitude of error. In this study the goal we try to achieve by avoiding oscillatory error is to reduce the magnitude of error.

It should also be pointed out that one can have several choices for providing values at the "ghost grid". For example, one might use

$$\phi_{N+1}^n = \phi_N^n, \phi_{N+1}^* = \phi_N^*. \tag{3.27}$$

Comparison of Figures 3.2 and 3.3 implies that the boundary condition (3.26) is better than (3.27).
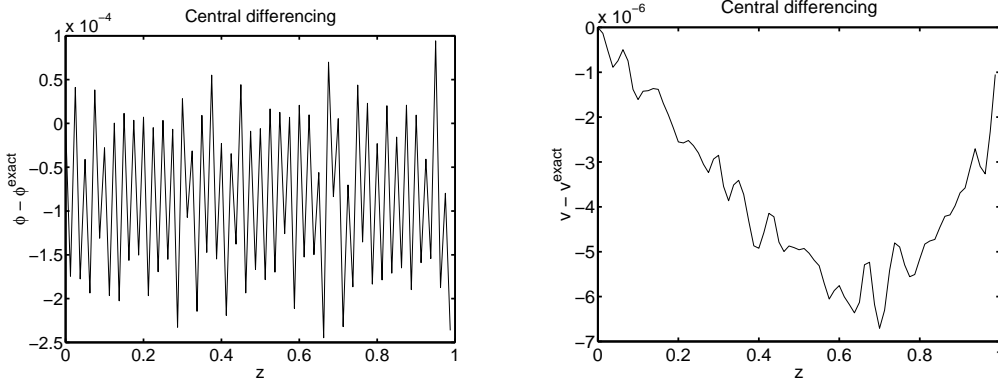

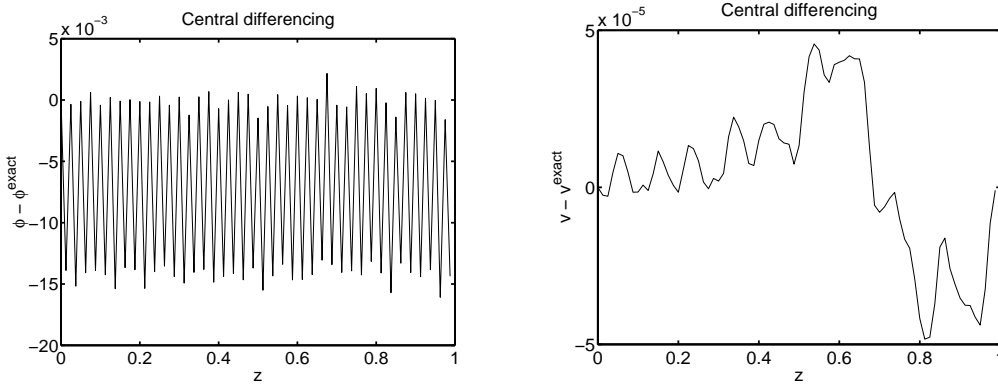FIG. 3.2. *Error of central differencing method using the boundary condition (3.26).*

FIG. 3.3. *Error of central differencing method using the boundary condition (3.27).*

"MacCormack" method

MacCormack's scheme [15] was originally developed for solving conservative hyperbolic equations. First it uses the one-sided first order scheme to obtain predicted values. Then it uses two-level points to approximate the spatial derivatives. In the first

level the upwind-like stencil is employed whereas in the second level the downwind-like stencil is used with the predicted values. Here we adopt the idea and obtain:

$$Predictor\colon \begin{cases} \phi_j^* = \phi_j^n - \dfrac{\Delta t}{\Delta z}[(\phi_j^n - \phi_{j-1}^n) + (v_j^n - v_{j-1}^n)] \\[2ex] v_j^* = v_j^n + \dfrac{\Delta t}{\Delta z}[(\phi_j^n - \phi_{j-1}^n) - (v_j^n - v_{j-1}^n)] + \dfrac{\Delta t}{(\Delta z)^2}(v_{j+1}^n - 2v_j^n + v_{j-1}^n) \end{cases} \quad (3.28)$$

$$Corrector\colon \begin{cases} \phi_j^{n+1} = \dfrac{\phi_j^n + \phi_j^*}{2} - \dfrac{\Delta t}{2\Delta z}[(\phi_{j+1}^* - \phi_j^*) + (v_{j+1}^* - v_j^*)] \\[2ex] v_j^{n+1} = \dfrac{v_j^n + v_j^*}{2} + \dfrac{\Delta t}{2\Delta z}[(\phi_{j+1}^* - \phi_j^*) - (v_{j+1}^* - v_j^*)] \\[2ex] \qquad\qquad + \dfrac{\Delta t}{2(\Delta z)^2}(v_{j+1}^* - 2v_j^* + v_{j-1}^*) \end{cases} \quad (3.29)$$

where $j = 2, \cdots, N$. The boundary conditions are

$$\phi_1^n = \phi_1^* = 1, v_1^n = v_1^* = 1, v_{N+1}^n = v_{N+1}^* = 1.5, \quad (3.30)$$

and

$$\phi_{N+1}^* = 2\phi_N^* - \phi_{N-1}^*. \quad (3.31)$$

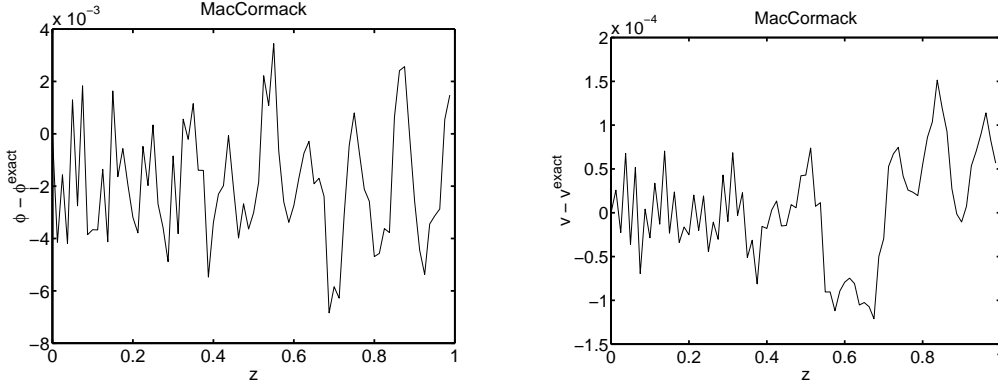Figure 3.4 gives the result using MacCormack's method with boundary conditions

FIG. 3.4. *Error of MacCormack method.*

(3.30) and (3.31). Again, initial conditions, mesh size and final time are the same as before. Evidently, MacCormack's method still cannot avoid oscillations.

So far, only the one-sided method does not exhibit oscillations. But the one-sided method is only first-order. Fiber specifications require sub-micron tolerances on radius fluctuations, so that it is desirable to use a high-order method. Furthermore, all the methods presented above are explicit and the stability condition requires that $\Delta t \le \min(C\Delta z/\max|v|, 0.5(\Delta z)^2)$ where C is the CFL constant. For moderately small

Δz, this method is very inefficient. To use a larger time step Δt, one has to exploit an implicit method. With these two things in mind, we propose a numerical method based on MacCormack's method, flux limiting [13] and the Crank-Nicolson method.

Modified MacCormack method with flux limiting

For hyperbolic systems, the flux limiter is usually imposed on characteristic variables. Because the PDE in our study (in the absence of viscosity) is elliptic everywhere, we simply impose the flux limiter on physical variables. Numerical results show that this is adequate for suppressing numerical oscillations. We apply limiters to the flux, not to the slope of variables [19]. More specifically, the flux of the first-order non-oscillatory method is

$$\text{flux}_1 = \phi^n + v^n, \tag{3.32}$$

whereas the flux of the (second-order) MacCormack method is

$$\text{flux}_2 = 0.5 * (\phi^* + v^* + \phi^n + v^n). \tag{3.33}$$

We rewrite flux_2 as

$$\text{flux}_2 = \text{flux}_1 + (\text{flux}_2 - \text{flux}_1), \tag{3.34}$$

and then apply limiters on the difference between two fluxes $(\text{flux}_2 - \text{flux}_1)$. This idea is the same as the approach used by Harten [11]. When applied to a scalar hyperbolic equation, the method is TVD.

Applying the above observation, we obtain the modified MacCormack method with flux limiting:

$$Predictor: \begin{cases} \phi_j^* = \phi_j^n - \dfrac{\Delta t}{\Delta z}[(\phi_j^n - \phi_{j-1}^n) + (v_j^n - v_{j-1}^n)] \\[3mm] v_j^* = v_j^n + \dfrac{\Delta t}{\Delta z}[(\phi_j^n - \phi_{j-1}^n) - (v_j^n - v_{j-1}^n)] + \dfrac{\Delta t}{(\Delta z)^2}(v_{j+1}^* - 2v_j^* + v_{j-1}^*) \end{cases} \tag{3.35}$$

$$Corrector: \begin{cases} \phi_j^{n+1} = \phi_j^n - \dfrac{\Delta t}{\Delta z}(f_{j+\frac{1}{2}} - f_{j-\frac{1}{2}}) \\[3mm] v_j^{n+1} = v_j^n + \dfrac{\Delta t}{\Delta z}(g_{j+\frac{1}{2}} - g_{j-\frac{1}{2}}) + \dfrac{\Delta t}{2(\Delta z)^2}(v_{j+1}^n - 2v_j^n + v_{j-1}^n) \\[3mm] \qquad + \dfrac{\Delta t}{2(\Delta z)^2}(v_{j+1}^{n+1} - 2v_j^{n+1} + v_{j-1}^{n+1}) \end{cases} \tag{3.36}$$

where $j = 2, \cdots, N$. The fluxes $f_{j+\frac{1}{2}}$ and $g_{j+\frac{1}{2}}$ are

$$f_{j+\frac{1}{2}} = \phi_j^n + v_j^n + \frac{\mathcal{A}\left(2[(\phi_j^* + v_j^*) - (\phi_{j-1}^n + v_{j-1}^n)], (\phi_{j+1}^* + v_{j+1}^*) - (\phi_j^n + v_j^n)\right)}{2}, \tag{3.37}$$

$$g_{j+\frac{1}{2}} = \phi_j^n - v_j^n + \frac{\mathcal{A}\left(2[(\phi_j^* - v_j^*) - (\phi_{j-1}^n - v_{j-1}^n)], (\phi_{j+1}^* - v_{j+1}^*) - (\phi_j^n - v_j^n)\right)}{2}, \tag{3.38}$$

where the special function $\mathcal{A}(x, y)$ is defined as

$$\mathcal{A}(x, y) = \begin{cases} x, \text{ if } x \cdot y \geq 0 \text{ and } |x| \leq |y| \\ y, \text{ if } x \cdot y \geq 0 \text{ and } |x| > |y| \\ 0, \text{ if } x \cdot y < 0. \end{cases} \tag{3.39}$$

Or in a more compact form, $\mathcal{A}(x,y)$ can be expressed as

$$\mathcal{A}(x,y) = \operatorname{sgn}(x)\max\left(0,\min(|x|,\operatorname{sgn}(x)\cdot y)\right). \tag{3.40}$$

Note that
- If the special function $\mathcal{A}(x,y)$ is identically zero, then we obtain the one-sided first order scheme;
- If $\mathcal{A}(x,y)$ is chosen by

$$\mathcal{A}(x,y) = y, \tag{3.41}$$

then one recovers MacCormack's scheme.

The boundary conditions are

$$\phi_1^n = \phi_1^{n+1} = 1, v_1^n = v_1^* = v_1^{n+1} = 1, v_{N+1}^n = v_{N+1}^* = v_{N+1}^{n+1} = 1.5, \tag{3.42}$$

and

$$\phi_{N+1}^* = 2\phi_N^* - \phi_{N-1}^*. \tag{3.43}$$

To find v^*, one needs to solve a tridiagonal system (which can be solved using Crout factorization method). Similarly, v^{n+1} is obtained by solving another tridiagonal system. Now the stability condition is given by the CFL condition only: $\Delta t \le C\Delta z/\max|v|$ where C is the CFL constant.

In Figure 3.5 we plot the error of the modified MacCormack method with flux limiting. All the numerical parameters remain the same as before. Clearly, this method does not generate oscillations while still maintaining high accuracy.
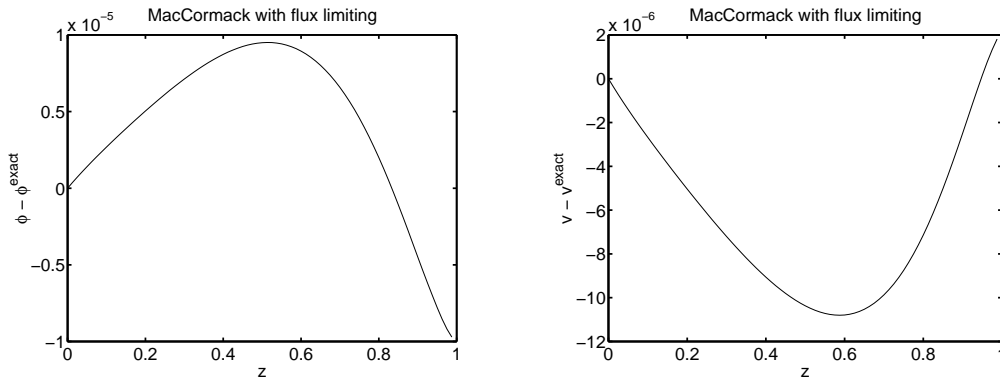

FIG. 3.5. *Error of modified MacCormack method with flux limiting.*

4. Numerical method for solving glass fiber equations

In this section we extend the modified MacCormack method with flux limiting to solve the glass fiber equations (2.1). For glass fibers, viscosity is usually very large. We find that the Crank-Nicolson method does not completely suppress small amplitude numerical oscillations. This is because the Crank-Nicolson method is not L-stable. To see this intuitively, consider the model ODE

$$y' = -\lambda y. \tag{4.1}$$

The amplification factor $\rho(\lambda)$ of the Crank-Nicolson method is

$$\rho(\lambda) = \frac{1 - \frac{\lambda}{2}\Delta t}{1 + \frac{\lambda}{2}\Delta t}, \tag{4.2}$$

$|\rho(\lambda)|$ does not go to zero when $\lambda\Delta t >> 1$.

To obtain L-stability, one can use a weighting scheme in the corrector step, as employed by Eggers and Dupont [5] for the isothermal limit of this model.

Introducing $u = \phi^2$, $w = \phi^2 v$, we rewrite (2.1) as

$$\begin{cases} u_t + w_z = 0, \\[2mm] w_t + (\dfrac{w^2}{u} - \dfrac{1}{W}\sqrt{u})_z = \dfrac{1}{F}u + [\eta(T)u(\dfrac{w}{u})_z]_z, \\[3mm] T_t + \dfrac{w}{u}T_z = \dfrac{H}{\sqrt{u}}(T_{wall}^4 - T^4) - \dfrac{2St}{u}[(\dfrac{w}{\sqrt{u}})^m](T - T_a). \end{cases} \tag{4.3}$$

The numerical scheme consists of two steps. In the first (predictor) step, for $j = 2, \cdots, N$, one has

$$u_j^* = u_j^n - \frac{\Delta t}{\Delta z}(f_{j+\frac{1}{2}} - f_{j-\frac{1}{2}}), \tag{4.4}$$

$$\begin{aligned}
w_j^* = w_j^n &- \frac{\Delta t}{\Delta z}(g_{j+\frac{1}{2}} - g_{j-\frac{1}{2}}) + \frac{\Delta t}{F}u_j^n \\[2mm]
&+ \frac{\Delta t}{(\Delta z)^2}\left[\eta(\frac{T_{j+1}^n + T_j^n}{2})\frac{u_{j+1}^n + u_j^n}{2}\left(\frac{w_{j+1}^*}{u_{j+1}^n} - \frac{w_j^*}{u_j^n}\right)\right. \\[2mm]
&\left.- \eta(\frac{T_j^n + T_{j-1}^n}{2})\frac{u_j^n + u_{j-1}^n}{2}\left(\frac{w_j^*}{u_j^n} - \frac{w_{j-1}^*}{u_{j-1}^n}\right)\right],
\end{aligned} \tag{4.5}$$

$$\begin{aligned}
T_j^* = T_j^n &- \frac{\Delta t}{\Delta z}\frac{w_j^n}{u_j^n}(T_j^n - T_{j-1}^n) + \frac{H}{\sqrt{u_j^n}}[T_{wall}^4 - (T_j^n)^4]\Delta t \\[2mm]
&- \frac{2St}{u_j^n}\left[\frac{w_j^n}{\sqrt{u_j^n}}\right]^m (T_j^n - T_a)\Delta t,
\end{aligned} \tag{4.6}$$

where the flux functions are

$$f_{j+\frac{1}{2}} = w_j^n, \tag{4.7}$$

$$g_{j+\frac{1}{2}} = \frac{[w_j^n]^2}{u_j^n} - \frac{1}{W}\sqrt{u_j^n}. \tag{4.8}$$

The boundary conditions are:

$$\text{upstream:} \, u_1^n, w_1^n, T_1^n \text{ are given} \tag{4.9}$$

$$\text{downstream:} \begin{cases} \dfrac{w_{N+1}^n}{u_{N+1}^n} \equiv Dr \text{ is given} \\ w_{N+1}^n = 2w_N^n - w_{N-1}^n \\ u_{N+1}^n = w_{N+1}^n / Dr \\ T_{N+1}^n = 2T_N^n - T_{N-1}^n \end{cases} \tag{4.10}$$

In the second (corrector) step, we update w first and then use the new values of w rather than the predicted values of w to update u. This treatment seems more natural. Therefore, for $j = 2, \cdots, N$, we have

$$u_j^{n+1} = u_j^n - \frac{\Delta t}{\Delta z}(\tilde{f}_{j+\frac{1}{2}} - \tilde{f}_{j-\frac{1}{2}}), \tag{4.11}$$

$$w_j^{n+1} = w_j^n - \frac{\Delta t}{\Delta z}(\tilde{g}_{j+\frac{1}{2}} - \tilde{g}_{j-\frac{1}{2}}) + \frac{\Delta t}{2F}(u_j^n + u_j^*)$$

$$+ \frac{1+\epsilon}{2}\frac{\Delta t}{(\Delta z)^2}\left[\eta(\frac{T_{j+1}^* + T_j^*}{2})\frac{u_{j+1}^* + u_j^*}{2}\left(\frac{w_{j+1}^{n+1}}{u_{j+1}^*} - \frac{w_j^{n+1}}{u_j^*}\right)\right.$$

$$\left. - \eta(\frac{T_j^* + T_{j-1}^*}{2})\frac{u_j^* + u_{j-1}^*}{2}\left(\frac{w_j^{n+1}}{u_j^*} - \frac{w_{j-1}^{n+1}}{u_{j-1}^*}\right)\right]$$

$$+ \frac{1-\epsilon}{2}\frac{\Delta t}{(\Delta z)^2}\left[\eta(\frac{T_{j+1}^n + T_j^n}{2})\frac{u_{j+1}^n + u_j^n}{2}\left(\frac{w_{j+1}^n}{u_{j+1}^n} - \frac{w_j^n}{u_j^n}\right)\right.$$

$$\left. - \eta(\frac{T_j^n + T_{j-1}^n}{2})\frac{u_j^n + u_{j-1}^n}{2}\left(\frac{w_j^n}{u_j^n} - \frac{w_{j-1}^n}{u_{j-1}^n}\right)\right] \tag{4.12}$$

$$T_j^{n+1} = T_j^n - \frac{\Delta t}{2\Delta z}\frac{w_j^n}{u_j^n}(T_j^n - T_{j-1}^n) - \frac{\Delta t}{2\Delta z}\frac{w_j^{n+1}}{u_j^{n+1}}(\tilde{h}_{j+\frac{1}{2}} - \tilde{h}_{j-\frac{1}{2}})$$

$$+ \frac{H}{2\sqrt{u_j^n}}[T_{wall}^4 - (T_j^n)^4]\Delta t + \frac{H}{2\sqrt{u_j^{n+1}}}[T_{wall}^4 - (T_j^*)^4]\Delta t$$

$$- \frac{St}{u_j^n}\left[\frac{w_j^n}{\sqrt{u_j^n}}\right]^m (T_j^n - T_a)\Delta t - \frac{St}{u_j^{n+1}}\left[\frac{w_j^{n+1}}{\sqrt{u_j^{n+1}}}\right]^m (T_j^* - T_a)\Delta t, \tag{4.13}$$

where

$$\tilde{f}_{j+\frac{1}{2}} = w_j^n + \frac{\mathcal{A}\left(2(w_j^{n+1} - w_{j-1}^n), (w_{j+1}^{n+1} - w_j^n)\right)}{2}, \tag{4.14}$$

$$\tilde{g}_{j+\frac{1}{2}} = \frac{[w_j^n]^2}{u_j^n} - \frac{1}{W}\sqrt{u_j^n} + \frac{\mathcal{A}(2x, y)}{2}, \tag{4.15}$$

$$x = \left(\frac{[w_j^*]^2}{u_j^*} - \frac{1}{W}\sqrt{u_j^*}\right) - \left(\frac{[w_{j-1}^n]^2}{u_{j-1}^n} - \frac{1}{W}\sqrt{u_{j-1}^n}\right), \tag{4.16}$$

$$y = \left(\frac{[w_{j+1}^*]^2}{u_{j+1}^*} - \frac{1}{W}\sqrt{u_{j+1}^*}\right) - \left(\frac{[w_j^n]^2}{u_j^n} - \frac{1}{W}\sqrt{u_j^n}\right), \tag{4.17}$$

$$\tilde{h}_{j+\frac{1}{2}} = T_j^n + \mathcal{A}\left(2(T_j^* - T_{j-1}^n), (T_{j+1}^* - T_j^n)\right), \tag{4.18}$$

and $\mathcal{A}(\cdot, \cdot)$ is defined in (3.40). In (4.12), ϵ is a free parameter between 0 and 1. If ϵ is 0, then one obtains the second-order Crank-Nicolson method; if ϵ is 1, then one has a complete implicit first order method.

5. Order of spatial convergence

In this section we want to check the order of convergence in the spatial direction.

Recall that the L_1, L_2, and L_∞-norms for a vector $\mathbf{u} = (u_1, \cdots, u_N)$ on the uniform grid with mesh size $\frac{1}{N}$ are defined respectively by

$$||\mathbf{u}||_1 = \frac{\sum_{i=1}^N |u_i|}{N}, ||\mathbf{u}||_2 = \sqrt{\frac{\sum_{i=1}^N u_i^2}{N}}, ||\mathbf{u}||_\infty = \max_{1 \le i \le N} |u_i|. \tag{5.1}$$

In Tables 5.1 – 5.3 we check the order of convergence of our method in different norms as defined above. In this computation, $1/F = 1/W = 1$, $H = 0.2$, $St = 0.1$, $m = 1/3$, $T_a = 0.6$, $\eta(T) = 30.0$, $Dr = 5$, $\epsilon = 0.3$, and the final time is 10. As shown here, our method exhibits second-order accuracy in the spatial direction.

Notice that in the above computations, the viscosity is a constant. Now we keep all the other parameters unchanged but replace the constant viscosity by a typical temperature-dependent form,

$$\eta(T) = \exp[30\left(\frac{1}{T} - 1.0113\right)]. \tag{5.2}$$

The results are shown in Tables 5.4 – 5.6. Again, our method exhibits second-order accuracy.

6. Numerical experiments near the onset of linearized instability

In this section we want to further demonstrate the efficiency of our numerical scheme by benchmarking the code at the onset of controllable instability.

In [8] we have solved steady state boundary-value solutions for a more general class than (2.1), and performed the linearized stability analysis of steady state solutions by solving an eigenvalue problem. Those equations and codes contain the system (2.1) as a special case. Now we want to use results from [8] to test the performance of all

TABLE 5.1. *The order of convergence for radius ϕ where $\eta(T) = 30$.*

error of $||\phi||_1$	order	error of $||\phi||_2$	order	error of $||\phi||_\infty$	order
6.3848e-6 ♣		6.9867e-6 ♣		9.4746e-6 ♣	
1.4932e-6 ♢	2.0963	1.6292e-6 ♢	2.1004	2.2038e-6 ♢	2.1041
3.3929e-7 ♡	2.1378	3.6912e-7 ♡	2.1420	4.9553e-7 ♡	2.1529

♣ Using 20–40 grid points
♢ Using 40–80 grid points
♡ Using 80–160 grid points

TABLE 5.2. *The order of convergence for axial velocity v where $\eta(T) = 30$.*

error of $||v||_1$	order	error of $||v||_2$	order	error of $||v||_\infty$	order
4.9177e-5 ♣		5.7460e-5 ♣		8.9325e-5 ♣	
1.1685e-5 ♢	2.0734	1.3680e-5 ♢	2.0705	2.1489e-5 ♢	2.0555
2.7008e-6 ♡	2.1131	3.1754e-6 ♡	2.1070	5.0514e-6 ♡	2.0888

♣ Using 20–40 grid points
♢ Using 40–80 grid points
♡ Using 80–160 grid points

TABLE 5.3. *The order of convergence for temperature T where $\eta(T) = 30$.*

error of $||T||_1$	order	error of $||T||_2$	order	error of $||T||_\infty$	order
5.1560e-5 ♣		5.9112e-5 ♣		1.5000e-4 ♣	
1.2745e-5 ♢	2.0164	1.4009e-5 ♢	2.0771	3.7422e-5 ♢	2.0030
3.1637e-6 ♡	2.0102	3.4002e-6 ♡	2.0427	9.3428e-6 ♡	2.0020

♣ Using 20–40 grid points
♢ Using 40–80 grid points
♡ Using 80–160 grid points

TABLE 5.4. *The order of convergence for radius ϕ where $\eta(T) = exp[30(1/T - 1.0113)]$.*

error of $||\phi||_1$	order	error of $||\phi||_2$	order	error of $||\phi||_\infty$	order
4.0910e-4 ♣		6.0634e-4 ♣		1.3571e-3 ♣	
1.0646e-4 ♢	1.9422	1.5561e-4 ♢	1.9622	3.5159e-4 ♢	1.9486
2.6674e-5 ♡	1.9968	3.8801e-5 ♡	2.0037	8.7929e-5 ♡	1.9995

♣ Using 20–40 grid points
♢ Using 40–80 grid points
♡ Using 80–160 grid points

TABLE 5.5. *The order of convergence for axial velocity v where $\eta(T) = exp[30(1/T - 1.0113)]$.*

error of $||v||_1$	order	error of $||v||_2$	order	error of $||v||_\infty$	order
3.8444e-3 ♣		4.8094e-3 ♣		8.3349e-3 ♣	
9.8634e-4 ♢	1.9626	1.2285e-3 ♢	1.9689	2.1280e-3 ♢	1.9696
2.4641e-4 ♡	2.0010	3.0647e-4 ♡	2.0031	5.3067e-4 ♡	2.0036

♣ Using 20–40 grid points
♢ Using 40–80 grid points
♡ Using 80–160 grid points

TABLE 5.6. *The order of convergence for temperature T where $\eta(T) = exp[30(1/T - 1.0113)]$.*

error of $||T||_1$	order	error of $||T||_2$	order	error of $||T||_\infty$	order
1.2993e-4 ♣		1.3518e-4 ♣		2.0141e-4 ♣	
3.4855e-5 ♢	1.8983	3.5774e-5 ♢	1.9179	5.1752e-5 ♢	1.9604
8.9214e-6 ♡	1.9660	9.1058e-6 ♡	1.9740	1.3038e-5 ♡	1.9888

♣ Using 20–40 grid points
♢ Using 40–80 grid points
♡ Using 80–160 grid points

the above schemes and demonstrate that our proposed scheme gives the best results. The idea here is to benchmark the transient PDE code near the onset of linearized stability of boundary-value solutions. The precise question is whether the PDE code correctly indicates linearized growth of superimposed spatial perturbations on steady states, at the precise critical parameter value. We focus on variation of the take-up speed, for fixed upstream boundary conditions. Using the codes developed in [8], we
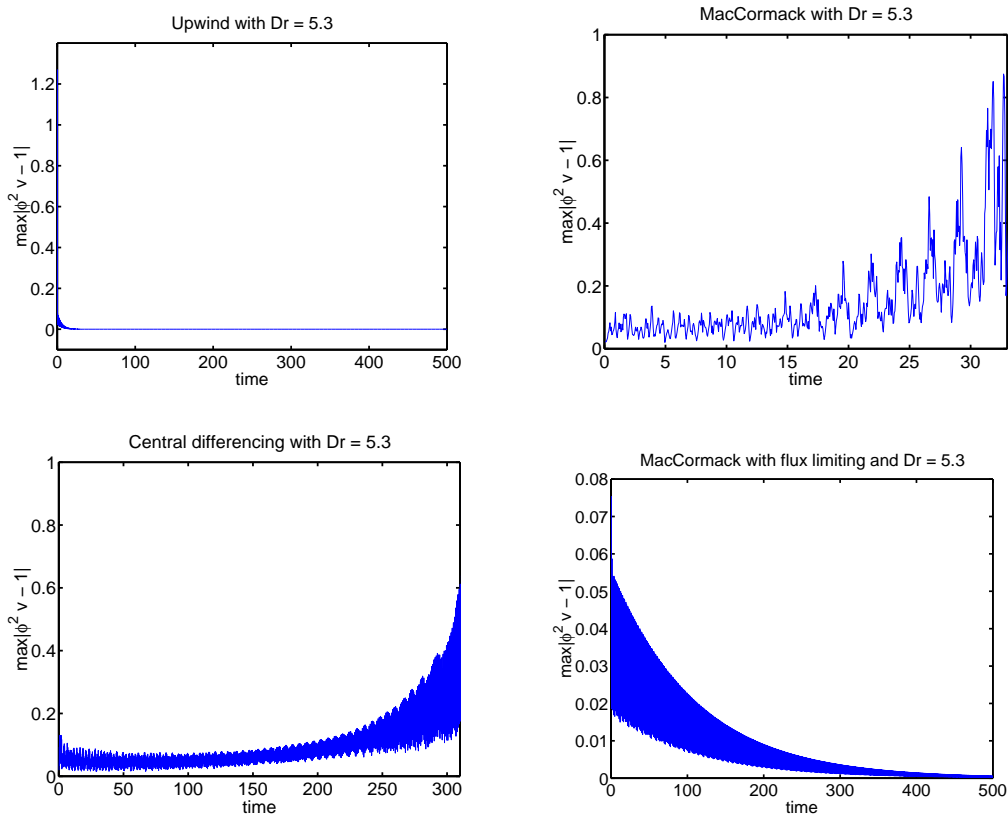

FIG. 6.1. *A comparison of the one-sided, MacCormack, central differencing and MacCormack with flux limiting schemes with Dr = 5.3.*

find that for the isothermal case where the temperature T is constant and $\eta(T) = 3$, and the other parameters are $1/F = 0$, $1/W = 10$, the critical draw ratio Dr^* – *the critical fiber spinning speed above which the steady state solution is linearly unstable*, is about 5.39. The value is obtained by solving an eigenvalue problem. Now we can initially perturb the steady state solutions with draw ratio equal to 5.3 ($< Dr^*$) and 5.5 ($> Dr^*$) respectively, and use the different numerical schemes discussed above to obtain the time-dependent solution. If the time-dependent solution relaxes to the steady state solution, then the critical draw ratio is predicted to be above the current draw ratio; otherwise, the critical draw ratio is lower.

Figure 6.1 demonstrates the results for $Dr = 5.3$. The one-sided first order scheme and the flux-limiting-MacCormack scheme both predict that the steady state is stable, whereas the MacCormack scheme and central differencing scheme imply that the
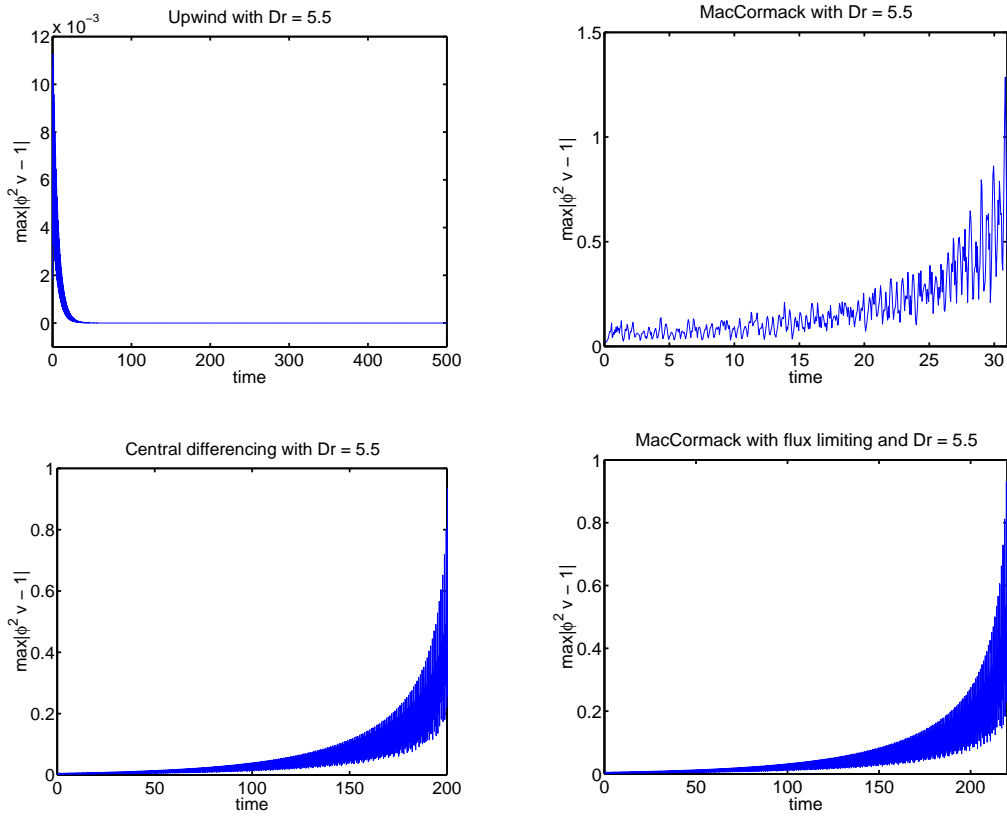
FIG. 6.2. *A comparison of the one-sided, MacCormack, central differencing and MacCormack with flux limiting schemes with Dr = 5.5.*

steady state is unstable. Figure 6.2 gives the results for $Dr = 5.5$. This time only the one-sided first order scheme predicts that the steady state is stable. The oscillations of the curves are consistent with nonzero imaginary parts of the largest-real-part linearized eigenvalue. As shown in Figures 6.1 and 6.2, the MacCormack and central differencing schemes both underestimate the critical draw ratio, whereas the one-sided first order scheme overestimates the critical draw ratio. **Only the flux-limiting-MacCormack scheme gives a prediction consistent with linearized stability analysis**.

7. Conclusions

In this paper we have presented an efficient numerical method for solving the governing model equations of a thermal glass fiber drawing process. Our method combines the MacCormack scheme from hyperbolic conservation laws with the ideas of flux limiting generally used in high resolution methods [11]. The method is tested on a linearized transient model and against a linearized boundary-value stability method. This method can now be applied to predict various aspects of the physical process [7]: confirmation of linearized stability; bounds on the domain of convergence for linearly stable solutions; and most importantly, spatial stability to transient perturbations at

boundaries, which is the primary source of fiber instability and which is unresolved by linearized stability methods.

REFERENCES

[1] S. E. Bechtel, M. G. Forest, Q. Wang and H. Zhou, *Free surface viscoelastic and liquid crystalline polymer fibers and jets,* invited chapter in the Elsevier Science Book series (Rheology Series), "Advances in the Flow and Rheology of Non-Newtonian Fluids", 1998.
[2] S. E. Bechtel, C. D. Carlson and M. G. Forest, *Recovery of the Rayleigh capillary instability from slender 1D inviscid and viscous models,* Phys. Fluids, 7, 2956-2971, 1995.
[3] A. N. Beris and B Liu, *Time dependent fiber spinning equations: 1. Analysis of mathematical behavior,* J. Non-Newtonian Fluid Mech., 26, 341-361, 1988.
[4] J. N. Dewynne, J. R. Ockendon and P. Wilmott, *On a mathematical model for fiber tapering,* SIAM J. Appl. Math., 49, 983-990, 1989.
[5] J. Eggers and T. F. Dupont, *Drop formation in a one-dimensional approximation of the Navier-Stokes equation,* J. Fluid Mech., 262, 205-221, 1993.
[6] M. G. Forest and Q. Wang, *Dynamics of slender viscoelastic free jets,* Siam J. Appl. Math., 54, 4, 996-1032, 1994.
[7] M. G. Forest and H. Zhou, *Unsteady analyses of thermal glass fibre drawing processes,* Euro. J. Appl. Math., 12, 479-496, 2001.
[8] M. G. Forest, H. Zhou and Q. Wang, *Thermotropic liquid crystalline polymer fibers,* SIAM J. Appl. Math., 60, 1177-1204, 2000.
[9] F. T. Geyling and G. M. Homsy, *Extensional instabilities of the glass fiber drawing process,* Glass Tech. 21, 2, 95-102, 1980.
[10] L. R. Glicksman, *The cooling of glass fibres,* Glass Tech., 9, 5, 131-138, 1968.
[11] A. Harten, *High resolution schemes for hyperbolic conservation laws,* J. Comp. Phys., 135, 2, 260-278, 1987.
[12] S. Jin, *Numerical integrations of systems of conservation laws of mixed type,* SIAM J. Appl. Math., 55, 1536-1551, 1995.
[13] R. J. LeVeque, *Numerical Methods for Conservation Laws,* Springer-Verlag, 1992.
[14] B. Liu and A. N. Beris, *Time dependent fiber spinning equations: 2. Analysis of mathematical behavior,* J. Non-Newtonian Fluid Mech., 26, 363-394, 1988.
[15] R. MacCormack, *Proceedings of the Second International Conference on Numerical Methods in Fluid Dynamics,* Lecture Notes in Physics, Springer-Verlag, New York, 8, 1971.
[16] M. Myers, *A model for unsteady analysis of preform drawing,* AIChE J., 35, 4, 592-602, 1989.
[17] W. W. Schultz and S. H. Davis, *One-dimensional liquid fibers,* J. Rheol., 26, 331-345, 1982.
[18] L. Ting and J.B. Keller, *Slender jets and thin sheets with surface tension,* SIAM J. Appl. Math., 50, 1533-1535, 1990.
[19] B. Van Leer, *Toward the ultimate conservative difference schemes V: A second-order sequel to Godunov's method,* J. Comput. Phys., 32, 101-136, 1979.